

Neutron diffraction study of $\alpha\text{-MnC}_2\text{O}_4\cdot 2\text{D}_2\text{O}$

S. Mitsuda*

Institute for Solid State Physics, University of Tokyo, Tokyo 106, Japan

S. Simizu, J. Lukin, and S. A. Friedberg

Physics Department, Carnegie-Mellon University, Pittsburgh, Pennsylvania 15213

B. X. Yang[†] and G. Shirane

Brookhaven National Laboratory, Upton, New York 11973

(Received 14 March 1988)

A neutron diffraction study of $\alpha\text{-MnC}_2\text{O}_4\cdot 2\text{D}_2\text{O}$, a quasi-one-dimensional antiferromagnet with anisotropic interchain interactions, has been performed on powder specimens. It reveals two magnetically ordered phases at low temperatures. The upper phase below $T_N=2.4$ K has an incommensurate helical spin structure with propagation vector $\mathbf{Q}=(0.170, \frac{1}{2}, -0.025)$. A gradual transformation occurs below $T_2=1.5$ K, where a commensurate structure with a propagation vector $\mathbf{Q}=(0, \frac{1}{2}, 0)$ develops as the temperature falls, while evidence of the incommensurate structure diminishes.

INTRODUCTION

While ideal one-dimensional (1D) magnetic chain systems with only nearest-neighbor interactions should not show long-range order above $T=0$ K, real materials containing linear chains of magnetic atoms (quasi-1D systems) exhibit long-range order at nonzero temperatures due to weak interchain coupling. In the case where interchain interaction is strongly anisotropic, the physical properties of the system may be particularly interesting.¹ If all chains in the crystal are parallel and one interchain coupling is dominant, we may observe a crossover from 1D to 2D behavior before entering the 3D ordered state. It is also possible that the system will exhibit pronounced 2D character even in the 3D ordered state.

Recent neutron diffraction studies^{1,2} suggest that the quasi-one-dimensional antiferromagnet $\alpha\text{-FeC}_2\text{O}_4\cdot 2\text{D}_2\text{O}$ may exhibit such effects. The $\alpha\text{-FeC}_2\text{O}_4\cdot 2\text{D}_2\text{O}$ structure is shared by the hydrated or deuterated oxalates of several divalent transition metal ions. As shown in Fig. 1, the chemical unit cell contains four M^{2+} ions belonging to four different antiferromagnetic chains lying along the monoclinic b direction. As explained in conjunction with Table I, the symmetry of the structure is such that interchain interactions in the ordered state will be anisotropic. $\alpha\text{-FeC}_2\text{O}_4\cdot 2\text{D}_2\text{O}$ shows 3D order below $T_N=11.7$ K with doubling of the unit cell along the b axis, the chain direction. A discontinuous transition to a second magnetically ordered phase with additional doubling of the unit cell along the a axis was observed at $T_2=9.5$ K. Simizu *et al.*¹ noted that very little energy is involved in this transition, as indicated by the extremely small heat capacity anomaly found at T_2 . This is consistent with the presence even in the 3D ordered state of 2D antiferromagnetic sheets parallel to the (100) plane which interact only weakly with one another. Heat capacity data³

over a wider range above and below T_N also appear to support this picture.

The interactions in $\alpha\text{-FeC}_2\text{O}_4\cdot 2\text{D}_2\text{O}$ are Ising-like, and 1D and 2D Ising models have been used with some success^{3,4} to explain its magnetic and thermal properties. The isostructural compound $\alpha\text{-MnC}_2\text{O}_4\cdot 2\text{D}_2\text{O}$, on the

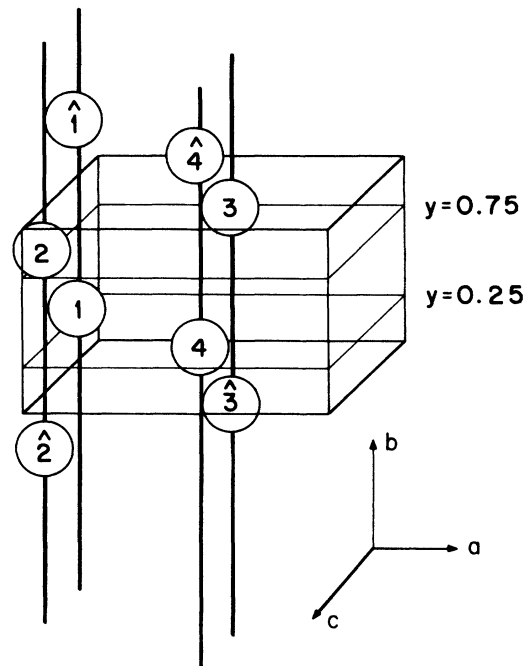


FIG. 1. The chemical unit cell for the $\alpha\text{-MnC}_2\text{O}_4\cdot 2\text{D}_2\text{O}$ structure. The four atoms in the unit cell belong to four different linear chains parallel to the monoclinic b axis. In the case of $\alpha\text{-MnC}_2\text{O}_4\cdot 2\text{D}_2\text{O}$, the Mn atoms lie close to but not exactly in the $y = \frac{1}{4}$ or $\frac{3}{4}$ planes.

TABLE I. Lattice constants and atomic positions in $\alpha\text{-MnC}_2\text{O}_4\cdot 2\text{D}_2\text{O}$. Atomic positions are shown for $T = 8$ K. Standard deviations are given in parentheses and apply to the least significant digits. Four Mn positions (4e) in a unit cell are (1) $(0, y, \frac{1}{4})$, (2) $(0, 1-y, \frac{3}{4})$, (3) $(\frac{1}{2}, \frac{1}{2} + y, \frac{1}{4})$, (4) $(\frac{1}{2}, \frac{1}{2} - y, \frac{3}{4})$. Monoclinic $\alpha\text{-MnC}_2\text{O}_4\cdot 2\text{D}_2\text{O}$ belongs to the space group $C2/c$. The site created by a primitive translation of site (n) along the b axis is labeled (\hat{n}), e.g., ($\hat{1}$) = $(0, 1 + y_0, \frac{1}{4})$ (see Fig. 1). The spins on sites (n) and (\hat{n}) are coupled antiferromagnetically by superexchange interaction via oxalate bridges along the b axis. Due to symmetry, nearest-neighbor interchain exchange interactions in the (001) plane cancel. For example, exchange interaction of site (3) [(4)] with site (1) [(2)] cancels that with site ($\hat{1}$) [($\hat{2}$)].

| T [K] | a (Å) | b (Å) | c (Å) | β | R factor |
|---------|-----------|----------|----------|------------|------------|
| 300 | 11.965(3) | 5.647(1) | 9.980(2) | 128.30°(1) | 0.117 |
| 8 | 11.710(3) | 5.656(1) | 9.891(2) | 127.99°(1) | 0.145 |

| Atom | Position | x | y | z |
|----------------|----------|----------|----------|----------|
| Mn | 4e | 0 | 0.226(3) | 0.250 |
| C | 8f | 0.051(2) | 0.674(4) | 0.351(2) |
| O ₁ | 8f | 0.087(2) | 0.472(4) | 0.428(3) |
| O ₂ | 8f | 0.092(2) | 0.878(4) | 0.434(3) |
| Ow | 8f | 0.181(2) | 0.185(4) | 0.250 |
| D ₁ | 8f | 0.335(2) | 0.618(3) | 0.367(3) |
| D ₂ | 8f | 0.222(2) | 0.598(3) | 0.133(3) |

other hand, should have interionic interactions predominantly of the isotropic Heisenberg type. As shown in Fig. 2, magnetic heat capacity data³ on this system above 4 K are well reproduced by the antiferromagnetic Heisenberg linear chain model with $S = \frac{5}{2}$ and $J/k = -1.17$ K. Also evident in these data (see inset in Fig. 2) are a small λ -type peak at $T_N = 2.4$ K and a second small but discernible anomaly at $T_2 = 1.5$ K. Below T_N , the magnetic heat capacity varies as T^2 and is reproduced by a noninteracting spin-wave calculation for a rectangular Heisenberg antiferromagnet with $|J'/J| = 0.02$. This suggests

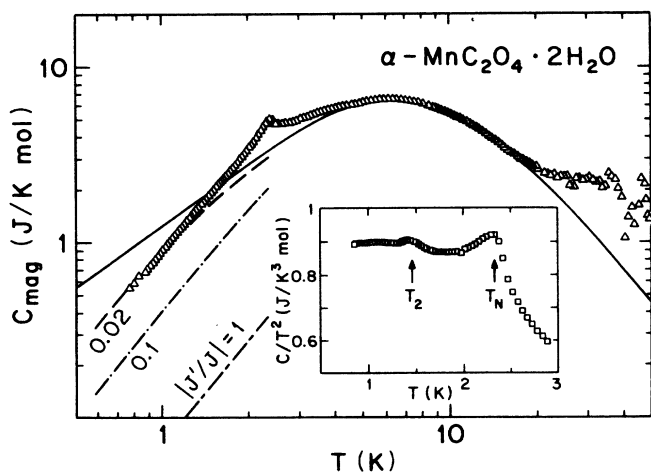


FIG. 2. Molar magnetic specific heat of $\alpha\text{-MnC}_2\text{O}_4\cdot 2\text{H}_2\text{O}$. Solid and dashed lines are calculated for the antiferromagnetic Heisenberg linear chain model with $S = \frac{5}{2}$ and $J/K = -1.17$ K and the rectangular Heisenberg antiferromagnet with anisotropic exchange $|J'/J| = 0.02$, respectively. The inset shows an enlarged plot of C_{mag}/T^2 vs T for the data below 3 K.

the existence in this system also of nearly independent 2D magnetic sheets even in the 3D ordered state. In this paper we wish to report the results of a neutron-diffraction study on powdered $\alpha\text{-MnC}_2\text{O}_4\cdot 2\text{D}_2\text{O}$ which confirms the ordering at $T_N = 2.4$ K and also reveals a second magnetically ordered phase below $T_2 = 1.5$ K.

Neutron diffraction measurements were carried out on the H4M triple axis spectrometer at the Brookhaven High Flux Beam Reactor. The (002) reflection of pyrolytic graphite (PG) was used for both monochromator and analyzer. A PG filter was used to remove higher order contamination from the beam. The collimation was $20' - 40' - 20' - 40'$ and the neutron wavelength 2.35 Å. Powder samples of $\alpha\text{-MnC}_2\text{O}_4\cdot 2\text{D}_2\text{O}$ were prepared by methods similar to those described in the literature⁵ for the hydrate.

EXPERIMENTAL RESULTS AND DISCUSSION

First we performed powder scans on $\alpha\text{-MnC}_2\text{O}_4\cdot 2\text{D}_2\text{O}$ at temperatures well above T_N , namely, 300 K and 8 K. Our results at 300 K gave lattice constants and atomic positions in good agreement with those found previously by x-ray diffraction on the hydrate.⁵ The same chemical structure with somewhat different lattice constants accounted for the data at 8 K. The results of applying Rietveld refinement methods⁶ to the 8 K data are shown in Table I. We have used the 8 K cell parameters in analyzing the magnetic structure at low temperatures. Powder scans in the range $5^\circ < 2\theta < 30^\circ$ were carried out at 3 K, 2 K, and 1.15 K, corresponding to high- ($T > 2.4$ K), intermediate- ($2.4 \text{ K} > T > 1.5$ K), and low-temperature ($1.5 \text{ K} > T$) phases, respectively. The results in the interval $10^\circ \leq 2\theta \leq 30^\circ$ are shown in Fig. 3.

Strong diffuse scattering was observed in the high-temperature phase, the integrated intensity of which

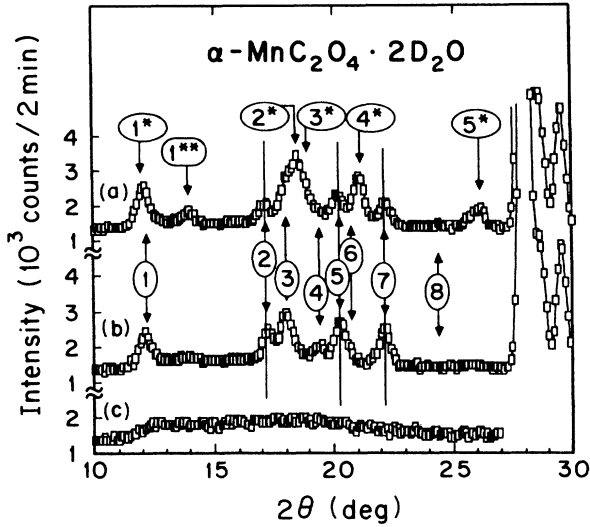


FIG. 3. Neutron diffraction pattern for powdered α - $\text{MnC}_2\text{O}_4 \cdot 2\text{D}_2\text{O}$ at (a) 1.15 K, (b) 2 K, and (c) 3 K. Sequential numbers in (a) and (b) correspond to those in Tables III and II, respectively.

reaches a maximum at $T_N = 2.4$ K, as shown in Fig. 4(b). In the intermediate phase the scattered intensity consists of diffuse scattering and magnetic Bragg peaks that are not commensurate with the chemical cell. These peaks are well explained by assuming a helical spin structure, to be discussed below, having a magnetic propagation vector $\mathbf{Q} = (0.170, \frac{1}{2}, -0.025)$. Calculated results for this structure are compared with the data in Table II. In the low-temperature phase, the scattering consists of reduced diffuse intensity and both incommensurate and commensurate Bragg peaks. As indicated in Fig. 3(a), the positions of the incommensurate peaks do not shift for $T < T_2$, although their overall intensity decreases in comparison with the $T = 2$ K values [Fig. 3(b)] as commensurate peaks appear.

Figure 4(a) shows the intensities of two incommensurate peaks growing from their initial appearance at T_N , reaching their maximum values at T_2 , and diminishing below that point. Also indicated is the growth in intensi-

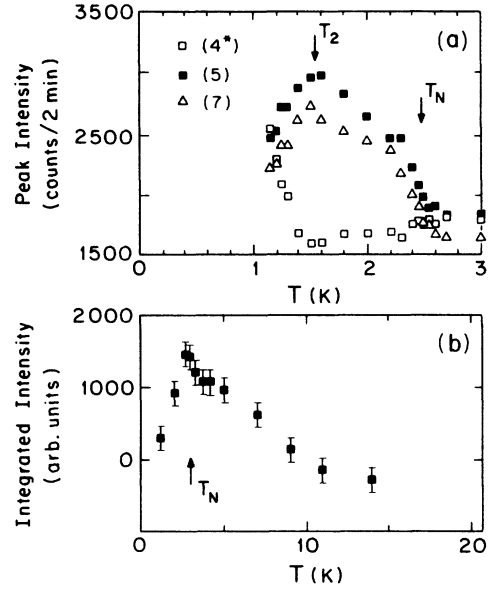


FIG. 4. Temperature dependence of (a) intensity of incommensurate and commensurate peaks, and (b) integrated intensity of diffuse scattering. The numbers (5), (7), and (4*) correspond to indices listed in Tables II and III.

ty of a commensurate peak as T falls below T_2 . The continuous transition at T_2 in the Heisenberg system α - $\text{MnC}_2\text{O}_4 \cdot 2\text{D}_2\text{O}$ is in marked contrast to the discontinuous transition between ordered magnetic phases previously observed^{1,3,4} in α - $\text{FeC}_2\text{O}_4 \cdot 2\text{D}_2\text{O}$ whose interactions are Ising-like.

The commensurate magnetic Bragg peaks have been indexed assuming doubling of the unit cell along the b axis. The integrated intensities of both incommensurate and commensurate magnetic Bragg peaks at 2 K and 1.15 K are listed in wavelength-independent form in Tables II and III, respectively. It should be noted that the commensurate intensity was obtained by subtracting scaled incommensurate data at 2 K from raw data at $T = 1.15$ K assuming that the structure factor for incommensurate peaks does not change with temperature. The nu-

TABLE II. Incommensurate magnetic peaks at $T = 2$ K. The squares of the structure factor have been calculated for the following configuration with an R factor of 14.3%: $\hat{n}_1^1 = \hat{n}_2^2 = -\hat{n}_3^3 = -\hat{n}_4^4$; $\hat{n}_3 = (-0.176, -0.321, 0.931)$ in Cartesian coordinates; $\phi^2 = 240^\circ$, $\phi^3 = 50^\circ$, $\phi^4 = 290^\circ$; $gS = 3.0\mu_B$; where we set $\phi^1 = 0^\circ$ because only relative phase angles have meaning.

| No. | Index | $2\theta_{\text{expt}}$ | $2\theta_{\text{calc}}$ | $ F_M ^2_{\text{expt}}$ (barn) | $ F_M ^2_{\text{calc}}$ (barn) |
|-----|-------------------------|-------------------------|-------------------------|--------------------------------|--------------------------------|
| (1) | $(0\bar{1}0) + Q$ | 12.1 | 12.15 | 0.38 | 0.38 |
| (2) | $(\bar{1}\bar{1}0) + Q$ | 17.2 | 17.26 | 0.82 | 1.06 |
| (3) | $(\bar{1}\bar{1}1) + Q$ | 18.0 | 18.01 | 1.40 | 1.49 |
| (4) | $(10\bar{1}) + Q$ | 19.35 | 19.47 | 0.39 | 0.45 |
| (5) | $(0\bar{1}\bar{1}) + Q$ | 20.25 | 20.31 | 1.67 | 1.53 |
| (6) | $(1\bar{1}0) + Q$ | | 20.74 | | 0.35 |
| (7) | $(0\bar{1}1) + Q$ | 22.15 | 22.14 | | 1.583 |
| (8) | $(\bar{2}\bar{1}1) + Q$ | | 24.39 | 0.0 | 0.29 |

TABLE III. Commensurate magnetic peaks at $T = 1.15$ K.

| No. | Index | $2\theta_{\text{calc}}$ | $2\theta_{\text{expt}}$ | $ F_M _{\text{expt}}^2$ |
|------|-------------------------|-------------------------|-------------------------|-------------------------|
| (1*) | $(0\frac{1}{2}0)$ | 11.94 | 12.0 | 0.32 |
| (2*) | $(1\frac{1}{2}\bar{1})$ | 18.62 | 18.5 | 3.06 |
| (3*) | $(1\frac{1}{2}0)$ | 18.94 | | |
| (4*) | $(0\frac{1}{2}1)$ | 21.13 | 21.1 | 2.28 |
| (5*) | $(2\frac{1}{2}\bar{1})$ | 26.17 | 26.15 | 1.36 |

clear reflections $(31\bar{2})$ and $(31\bar{1})$ were used to express the square of the magnetic structure factor in absolute units (barns). At present we do not understand the origin of the small peak (designated as 1** in Fig. 3) at $2\theta = 14^\circ$ which can be indexed as $(\frac{1}{2}\frac{1}{2}0)$. Further study is needed to clarify this point.

Let us consider now some details of a model which successfully explains the observations on the high-temperature ordered phase existing between T_N and T_2 . Attempts to extend this treatment to account for the behavior of $\alpha\text{-MnC}_2\text{O}_4 \cdot 2\text{D}_2\text{O}$ below T_2 are also described although, thus far, their success has been limited. We may write a general expression⁷ for the diffracted intensity from a conical spin structure in this system. The spin vector \mathbf{S}_j^l of the j th atom in the l th cell is given by

$$\mathbf{S}_j^l = S_{\parallel} [\hat{n}_1^j \cos(\mathbf{Q} \cdot \mathbf{R}^l + \phi^j) + \hat{n}_2^j \sin(\mathbf{Q} \cdot \mathbf{R}^l + \phi^j)] + S_{\perp} \hat{n}_3^j \cos(\mathbf{P} \cdot \mathbf{R}^l),$$

where \hat{n}_1^j , \hat{n}_2^j , and \hat{n}_3^j are orthogonal basis vectors that depend, in general, on site j in the unit cell. \mathbf{Q} is the propagation vector of the helix; ϕ^j is the initial phase of the helix measured from \hat{n}_1^j clockwise around \hat{n}_2^j . The third term represents a tilt of the moment from the helical plane and \mathbf{P} is the propagation vector for this component. The intensity then becomes

$$I \sim \sum_{\tau} \delta(\mathbf{k} - \tau - \mathbf{Q}) \mathbf{F}_+^* \cdot \mathbf{F}_+ + \sum_{\tau} \delta(\mathbf{k} - \tau + \mathbf{Q}) \mathbf{F}_-^* \cdot \mathbf{F}_- + \sum_{\tau} \delta(\mathbf{k} - \tau + \mathbf{P}) \mathbf{F}_z^* \cdot \mathbf{F}_z,$$

where

$$\mathbf{F}_{\pm}(\mathbf{k} = \tau \pm \mathbf{Q}) = (\gamma r_0) \frac{S_{\perp}}{2} f(\mathbf{k}) \sum_j \exp(i\mathbf{k} \cdot \mathbf{r}_j) \hat{\kappa} \times [\hat{\kappa} (\hat{n}_1^j \pm i\hat{n}_2^j)] \exp(\mp i\phi^j)$$

and

$$\mathbf{F}_z(\mathbf{k} = \tau + \mathbf{P}) = (\gamma r_0) S_{\perp} f(\mathbf{k}) \sum_j \exp(i\mathbf{k} \cdot \mathbf{r}_j) \hat{\kappa} \times (\hat{\kappa} \times \hat{n}_3^j).$$

\mathbf{F}_{\pm} and \mathbf{F}_z correspond to incommensurate and commensurate structure factors, respectively. τ is a reciprocal lattice vector for the chemical cell, $\hat{\kappa}$ is a unit vector along the scattering vector \mathbf{k} , and an asterisk identifies the complex conjugate of a given quantity. (γr_0) is a physical constant equal to 0.539×10^{-12} cm and $f(\mathbf{k})$ is the magnetic form factor of Mn^{2+} .

As indicated above, components of the spin perpendicular and parallel to \hat{n}_3^j give incommensurate and commensurate reflections, respectively. The incommensurate reflections should be determined, in general, by an eleven-parameter set $(\hat{n}_1^1, \dots, \hat{n}_3^4)$ setting $S_{\perp} = 0$. We have fitted the incommensurate data under the plausible constraint that all normal vectors \hat{n}_3^j for the helix sheet have the same axis. Even in this case \hat{n}_3^j may have two directions to signify the direction of helical rotation. Thus the following combinations are possible: $\hat{n}_3^1 = \hat{n}_3^2 = \hat{n}_3^3 = \hat{n}_3^4$, $\hat{n}_3^1 = \hat{n}_3^2 = \hat{n}_3^3 = -\hat{n}_3^4$, and so on. Good agreement with the data ($R = 14.3\%$) was obtained using the parameters listed in Table II. The sum of all calculat-

ed structure factors with the same $|\mathbf{k}|$ is given in Table II since $|F(hkl)|$ is not, in general, equal to $|F(\bar{h}\bar{k}\bar{l})|$. The value $gS = 3.0\mu_B$ at 2 K is quite reasonable since the extrapolated moment per Mn^{2+} ion at $T = 0$ K appears to be about $5\mu_B$.

A schematic drawing of the helical spin structure we are proposing for the high-temperature ordered phase of $\alpha\text{-MnC}_2\text{O}_4 \cdot 2\text{D}_2\text{O}$ is shown in Fig. 5. The structure represented by the above-mentioned \mathbf{Q} vector is one in which the spin direction changes antiferromagnetically along the b axis. This corresponds to the fact that the system consists basically of 1D antiferromagnetic chains parallel to that axis. The spin direction rotates incommensurately by $\sim 61^\circ$ along the a axis. Successive spins along what is essentially the c axis (neglecting the small number -0.025) are ferromagnetically aligned.

We have attempted to explain the temperature dependence of commensurate and incommensurate intensities below T_2 by assuming a conical structure in which the half-angle of the cone, $\tan^{-1}(S_{\parallel}/S_{\perp})$, becomes smaller as temperature decreases. Here we find $\mathbf{P} = (0\frac{1}{2}0)$ from the indices of the commensurate peaks listed in Table III. As seen in Fig. 4(a), the intensity ratio of two incommensurate peaks 5 and 7 does not vary even below T_1 . This suggests that the orientation of the normal vector \hat{n}_3^j

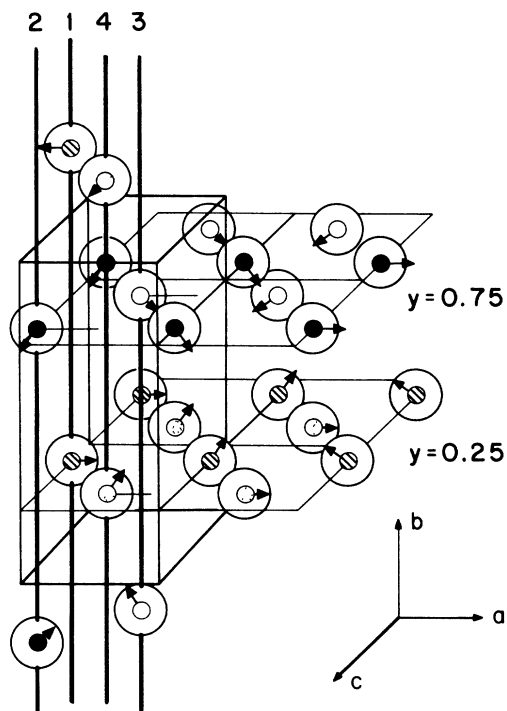


FIG. 5. Schematic drawing of the incommensurate spin structure of α - $\text{MnC}_2\text{O}_4 \cdot 2\text{D}_2\text{O}$ for $T_2 < T < T_N$. Mn atoms on site (1) [or (4)] and site (2) [or (3)] belong approximately to the planes with $y = 0.25$ and 0.75 , respectively.

remains the same. Besides, as already noted, the incommensurate intensity could be subtracted from the data at 1.15 K without assuming any change of the structure factor with temperature. Therefore, the commensurate peaks should be reproduced using the vector \hat{n}_3 obtained above. Here one notes that the sign of S_1 may take either positive or negative values because the conical collapse may occur in either direction normal to the helical plane. Although we tried all combinations, none yielded a reasonable solution. Thus our efforts to interpret the temperature dependence of the scattering below T_2 in terms of the gradual change from a helical to a collapsing conical structure have been unsuccessful to this point.

Another possible explanation of these data which suggests itself is a two-phase coexistence model. This would require a temperature-dependent fraction of the sample volume to possess a commensurate spin structure while the rest is incommensurate. These structures could presumably be described by the above-mentioned formalism using independent parameter sets. However, treating the system as inhomogeneous in this fashion appears to be too arbitrary and has not been attempted.

While this work has yielded a satisfactory interpretation of the ordered magnetic structure of α - $\text{MnC}_2\text{O}_4 \cdot 2\text{D}_2\text{O}$ between T_N and T_2 , it has not yet provided a consistent understanding of the behavior below T_2 . Nor is it yet possible to draw any conclusions about the suspected presence of pronounced 2D character in the 3D ordered state. Experiments on single crystals well below 1 K are probably needed. We are presently trying to grow crystals of α - $\text{MnC}_2\text{O}_4 \cdot 2\text{D}_2\text{O}$ suitable for such experiments.

Note added. Since this work was completed and submitted for publication, we have learned of another neutron diffraction study on α - $\text{MnC}_2\text{O}_4 \cdot 2\text{D}_2\text{O}$ by Sledzinska *et al.*⁸ The only diffraction spectrum they report showing magnetic ordering was taken at 1.5 K. They are evidently unaware of differences in the spin structure existing above and below that temperature. From their data they infer the existence of a conical spiral structure similar to the one we have considered for the phase below $T_2 = 1.5$ K in the above discussion and found to be unsatisfactory. Since the measurements of Sledzinska *et al.* do not extend below 1.5 K, the significance of their interpretation is unclear.

ACKNOWLEDGMENTS

We wish to thank Y. Endoh, H. Yoshizawa, and D. E. Cox for helpful discussions. This work was supported in part by the U.S.-Japan Cooperative Neutron Scattering Program. The work at Carnegie-Mellon University was supported by the National Science Foundation under Grant No. DMR 84-05833 and that at Brookhaven National Laboratory by the Division of Materials Science, U.S. Department of Energy, under Contract No. DE-AC02-76CH00016.

*Temporary address: Brookhaven National Laboratory, Upton, NY 11973.

†Also at Department of Physics, State University of New York at Stony Brook, Stony Brook, NY 11794.

¹S. Simizu, J.-Y. Chen, S. A. Friedberg, J. Martinez, and G. Shirane, *J. Appl. Phys.* **61**, 3420 (1987).

²I. Sledzinska, A. Murasik, and M. Piotrowski, *Physica* **138B**, 315 (1986).

³S. Simizu and S. A. Friedberg, *J. Appl. Phys.* **63**, 3557 (1988).

⁴J.-Y. Chen, S. Simizu, and S. A. Friedberg, *J. Appl. Phys.* **57**,

3338 (1985).

⁵A. Huizing, H. A. M. van Hal, W. Kwestroo, C. Langereis, and P. C. van Loosdregt, *Mater. Res. Bull.* **12**, 605 (1977), and earlier references cited therein.

⁶H. M. Rietveld, *J. Appl. Cryst.* **2**, 65 (1969).

⁷D. E. Cox, W. J. Takei, and G. Shirane, *J. Phys. Chem. Solids* **24**, 405 (1963).

⁸I. Sledzinska, A. Murasik, and P. Fischer, *J. Phys. C* **20**, 2247 (1987).